Rethinking Low-quality Optical Flow in Unsupervised Surgical Instrument Segmentation

Peiran Wu^{1*}, Yang Liu^{2*†}, Jiayu Huo², Gongyu Zhang², Christos Bergeles², Rachel Sparks², Prokar Dasgupta², Alejandro Granados², and Sebastien Ourselin²

University of Bristol, Bristol, UK
King's College London, London, UK

on23019@bristol.ac.uk, {yang.9.liu, firstname.lastname}@kcl.ac.uk

Abstract. Video-based surgical instrument segmentation plays an important role in robot-assisted surgeries. Unlike supervised settings, unsupervised segmentation relies heavily on motion cues, which are challenging to discern due to the typically lower quality of optical flow in surgical footage compared to natural scenes. This presents a considerable burden for the advancement of unsupervised segmentation techniques. In our work, we address the challenge of enhancing model performance despite the inherent limitations of low-quality optical flow. Our methodology employs a three-pronged approach: extracting boundaries directly from the optical flow, selectively discarding frames with inferior flow quality, and employing a fine-tuning process with variable frame rates. We thoroughly evaluate our strategy on EndoVis2017 VOS dataset and Endovis2017 Challenge dataset, where our model demonstrates promising results, achieving a mean Intersection-over-Union (mIoU) of 0.75 and 0.72, respectively. Our findings suggest that our approach can greatly decrease the need for manual annotations in clinical environments and may facilitate the annotation process for new datasets. The code is available at https://github.com/wpr1018001/Rethinking-Low-quality-Optical-Flow.git.

Keywords: Surgical instrument segmentation \cdot Unsupervised learning \cdot Low-quality optical flow.

1 Introduction

Instrument segmentation is the key in robotic-assisted surgeries, offering improved guidance and aiding decision-making. This task is also crucial for some other AI-driven surgical tasks, such as workflow recognition [11,10,17], action identification [15], and tracking [2].

While deep learning has progressed fully- [23,14,13,18,6] and semi-supervised [21,22] models, they rely heavily on manual annotations, which increases the

^{*} Equal contribution.

[†] Corresponding author. Email: yang.9.liu@kcl.ac.uk

workload and limits their application. Our focus is on unsupervised segmentation to support surgery understanding with no extra manual action.

Initial unsupervised efforts in surgical tasks tackled workflow analysis [1] and motion prediction [3] while Instrument segmentation has seen less exploration. Liu et. al. [9] used unsupervised techniques and basic cues for segmentation. However, this approach's reliance on specific signals limits its adaptability across surgeries.

Motion, essential for visual processing, is leveraged in unsupervised models like RAFT [19] to capture movement in videos effectively. Sestini et. al. [16] introduced FUN-SIS, integrating realistic instrument segmentation masks (referred to as *shape-priors*) sourced from various datasets with optical flow information. Despite its novelty, FUN-SIS's dependency on the *shape-priors* and its non-end-to-end nature limited its application. Recently, Lian et. al. [7] brought forward RCF, a wholly unsupervised model for video object segmentation (VOS), showcasing the critical role of motion. The success of this model underlines the importance of optical flow quality in unsupervised learning, setting a new benchmark for instrument segmentation without manual annotations.

Unlike the high-quality optical flow found in natural videos, surgical footage often shows low quality due to challenges such as dark areas, abrupt movements, and stationary instruments, as shown in Figure 1. Following the approach of the RCF model [7], we aim to reduce the impact of low-quality optical flow on our model. Liao et al. [8] highlighted the importance of segmenting boundaries clearly, a task made difficult by the often blurred boundaries in surgical optical flow. Drawing on the method used in Super-BPD [20], we use angular measurements to detect these boundaries in the flow, ensuring our model focuses only where it's most reliable. Moreover, the frequent presence of low-quality optical flow in surgery videos poses a notable challenge. To tackle this, we drop the most difficult samples in each batch. Additionally, the subtle movement of some tools, barely captured by optical flow, can lead to model insensitivity. By varying frame rates beyond the standard, we improve the detection of these less visible movements.

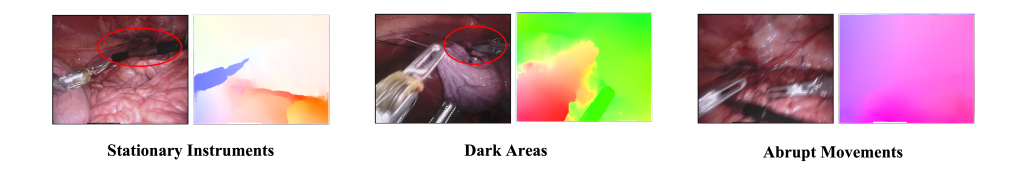


Fig. 1. Example of some low-quality optical flow frames, including stationary instruments, dark areas and abrupt movements, which greatly limit the model performance.

2 Method

We target the challenge of unsupervised surgical instrument segmentation within a video stream of T frames, denoted as $X_T = \{x_i | i \in \{1, ..., T\}\}$, where x_i represents the image of the i-th frame. The objective is to create a mapping function f such that $f(x_i)$ produces a mask that extracts the area of the surgical instrument. It is important to note that instrument mask annotations are not employed during the training stage.

For the backbone model, we use the first stage of the state-of-the-art (SOTA) model RCF [7] due to its independence from additional annotations like *shape-priors* and its excellence as an end-to-end model. Nonetheless, the quality of optical flow in surgical videos often suffers due to various factors, including areas of darkness, abrupt movements, and the presence of stationary instruments, as highlighted in Figure 1. To mitigate these issues, our approach introduces enhancements in three key areas: establishing a reliable boundary supervision mechanism, implementing a strategic frame-dropping strategy, and adopting variable frame rates for input during training. The detailed architecture of our proposed method is illustrated in Figure 2.

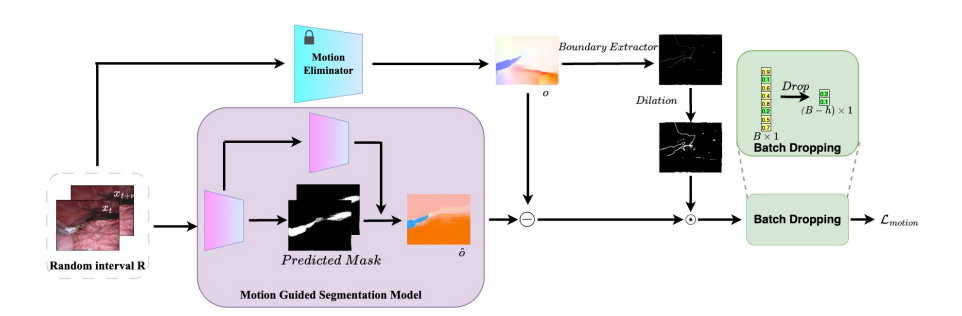


Fig. 2. The overview of our proposed unsupervised segmentation method. Two frames, separated by a random interval R, are fed into the model. A pre-trained optical flow estimator generates the pseudo labels (o) and a motion-guided segmentation model predicts optical flow (\hat{o}) by computing the segmentation map. Optical flow o processing by boundary detection and dilation to delineate areas for dependable supervision. Batch dropping is subsequently applied to select the most reliable frames.

2.1 Robust Boundary Supervision

The ability to capture instrument motion via optical flow is fundamental to conducting unsupervised instrument segmentation. However, the optical flow representation often fails to adequately describe surgical instruments due to limitations such as dark areas within the image and the presence of stationary instruments, as illustrated in Figure 1. Such restrictions on supervision can lead to poorer segmentation performance. Our investigations have revealed that the areas near boundaries depicted in optical flow tend to be more accurate than others, prompting the segmentation model to concentrate more on these boundary regions. Consequently, we introduce a boundary-nearby area supervision mechanism to leverage this observation for improved segmentation accuracy.

Initially, we transform the optical flow representation $o_i \in \mathbb{R}^{H \times W \times 2}$, encoding motion vectors in two dimensions (horizontal and vertical movements), into a directional format $\theta_i \in \mathbb{R}^{H \times W}$, where H and W represent the height and width of the image frame, respectively. This conversion calculates the angle θ_i^p of the optical flow at each pixel position p = (j, k). Specifically, the direction angle θ_i^p at position p is obtained through the formula:

$$\theta_i^p = \arctan 2(o_i^{j,k,x}, o_i^{j,k,y}),$$

where $o_i^{j,k,x}$ and $o_i^{j,k,y}$ are the horizontal and vertical components of the optical flow vector at the pixel p, respectively. Next, we define the directional difference at each pixel p as follows:

$$\delta_i^p = \max_{n^p \in \mathcal{N}_1^p} |\theta_i^p - \theta_i^{n^p}|,$$

where \mathcal{N}_1^p signifies the 4-neighbourhood of pixel p, including the adjacent pixels in both the vertical and horizontal orientations. To demarcate boundary regions, we introduce a difference threshold $\alpha = \frac{\pi}{12}$. This leads to the creation of the boundary mask M_i , where a value of 1 is assigned to pixels that meet the condition $\delta_i^p > \alpha$, indicating the presence of a boundary, while a value of 0 denotes areas without boundaries. To enhance the supervision diversity, a simple dilation technique is employed to broaden the areas under supervision. Specifically, for every boundary pixel satisfying $\delta_i^p > \alpha$, we set $M_i(\mathcal{N}_d^p)$ to 1, where d represents the dilation distance. This adjustment ensures that a more comprehensive non-boundary area can also be incorporated into the learning process. Consequently, the optical flow loss at each pixel p can be updated as:

$$\mathcal{L}(p) = M_i(p) \cdot ||o_i(p) - \hat{o}_i(p)||^2.$$

2.2 Batch Frame Dropping

We observed that the issue of low-quality optical flows predominantly manifests at the image level rather than being confined to specific areas, indicating that instances of low local optical flow quality often coincide with the overall inferior quality of the optical flow across the entire image. To address this challenge, we have devised a frame-level drop mechanism. Specifically, when processing a batch of B training images, we choose to exclude the lowest h hard cases, identified based on their loss values. This approach allows us to eliminate instances of low-quality optical flow, thereby enhancing the reliability of frame-level supervision.

2.3 Variable Frame Rates Training Input

Despite establishing reliable supervision mechanisms, instruments that frequently remain stationary pose a challenge to effective training due to the scarcity of meaningful optical flow supervision samples in these regions. To overcome this limitation, we introduce a strategy of feeding training images with variable frame rates, (x_i, x_{i+r}) , where the interval between adjacent frames, r, is a random number within the range of 1 to 3, instead of being fixed at r = 1. This variability ensures that the optical flow can capture the motion of instruments that typically exhibit little or no movement, thereby facilitating more effective training.

3 Experiments

3.1 Datasets and Evaluation Metrics

For our experimental analysis, we used datasets from the MICCAI EndoVis 2017 Robotic Instrument Segmentation Challenge. This dataset features 8 sets, each with 225 frames of stereo camera footage recorded by the da Vinci Xi surgical robot during various pig surgery procedures. Each frame has been meticulously annotated by experts, identifying distinct parts of robotic surgical instruments, categorizing them into rigid axes, articulated wrists, grommets, and a miscellaneous category for additional instruments like laparoscopic tools or drop-in ultrasound probes. We explored two variations of the EndoVis 2017 dataset for our study: EndoVis 2017 VOS and EndoVis 2017 Challenge. The VOS version includes laparoscopic tools and ultrasound probes as per Sestini et al. [16], while the Challenge version adheres to the original competition guidelines by excluding the 'other label' category. In the evaluation, we followed the same conventions and the same data partitioning and performed a 4-fold cross-validation on both the VOS and the challenge versions of the dataset [6]. Our primary evaluation metric is the mean Intersection-over-Union (mIoU), consistent with the benchmarks set in the MICCAI EndoVis 2017 Challenge and subsequent research in the field.

3.2 Implementation Details

For our model, we chose the RCF framework [7] as our backbone, leveraging a ResNet50 [5] for feature extraction, which feeds into both a segmentation and a residual prediction head. The optical flow is derived using the RAFT model, pretrained on synthetic datasets FlyingChairs [4] and FlyingThings [12], without any human-annotated data. Our implementation is based on PyTorch and runs on a single NVIDIA A100-PCIE-40GB GPU. We maintain a batch size of 8, applying the h=6 hard cases to ensure frame-level supervision quality. For boundary dilation, a kernel size of d=7 is used.

Table 1. Comparison with SOTA supervised methods and unsupervised methods. Mean IoU (%) is reported. And the results of prior works are quoted.

Annotation	Shape-priors	Stage	Method	EndoVis 2017VOS E	IndoVis 2017Challenge
100%	No	1	TernausNet [18]	89.06	83.60
100%	No	1	MF-TAPNet [6]	89.61	87.56
0%	Yes	1	FUN-SIS(Stage1)	40.08	37.03
0%	Yes	2	FUN-SIS(Stage2)	74.78	68.31
0%	Yes	3	FUN-SIS(Stage3)[16]	83.77	76.25
0%	No	1	AGSD [9]	71.47	67.85
0%	No	1	RCF(Stage1)	46.09	46.17
0%	No	2	RCF(Stage2)[7]	49.18	49.19
0%	No	1	RCF(Stage1) + Ours	75.07	72.07

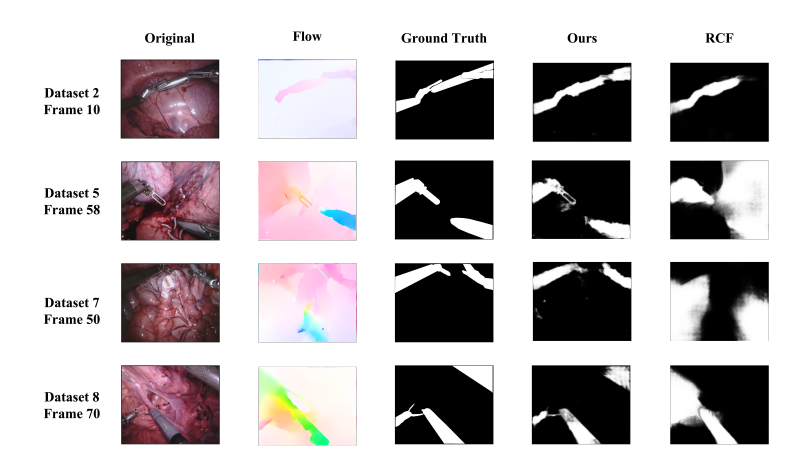


Fig. 3. Qualitative comparisons with the baseline model RCF, showing (a) optical flow pseudo-labels obtained by RAFT prediction (b) Ground Truth from EndoVis 2017, offering (c) Prediction masks of our method (d) Prediction masks of RCF.

3.3 Comparison with State-of-the-art Methods

Our findings on the EndoVis 2017 VOS and EndoVis 2017 Challenge datasets are presented in Table 1. We compare our method with the AGSD [9] and FUN-SIS [16] methods, both tailored to surgical video segmentation, and RCF [7], originally designed to segment natural images. Our method advances the RCF model, delivering an end-to-end solution without relying on *shape-priors* for annotations. The enhancements we have implemented lead to substantial performance enhancements, showing a 28.98 percentage points (pp) and 25.93 pp increase over the original RCF model on the EndoVis 2017 VOS and Challenge datasets, respectively. This confirms our approach's capability to refine the use of low-quality optical flow. Moreover, when measured against AGSD, our fully unsupervised method shows gains of 3.6 pp and 4.22 pp for the respective datasets, marking the first instance of a purely unsupervised model using optical flow out-

performing those dependent on crafted pseudo-labels. Our model also shows an edge over the FUN-SIS's second stage, surpassing it by 0.29 pp and 3.76 pp on the VOS and Challenge versions, respectively.

Figure 3 showcases comparative visual examples between our method and the baseline RCF model. Although RCF struggles with the typically low optical flow in surgical videos, our model excels, showing impressive results even in areas with challenging flow conditions. Particularly in detailed areas, such as the instrument head at case frame 58, our approach not only matches but also surpasses the ground truth.

3.4 Ablation Study

To ensure fairness and generalisability of results, in all our experiments we are using a 4-fold cross-validation on the EndoVis 2017 VOS dataset. We performed exhaustive ablation experiments on functions such as Batch frame dropping (Dropping), Robust Boundary Supervision (Boundary) and Variable frame rates training input (Variable).

Different Components of Method. We conduct experiments to analyze the effects of different components of our method. Specifically, our method contains three parts: Dropping, Boundary and Variable. To increase the readability of the form, we use check marks to mark whether or not a function is used. Based on Table 2, we can clearly see that: (1) Baseline Performance: Initially, the model's mIoU stands at 46.09% without the implementation of any specific strategies, serving as the baseline for comparison. (2) Impact of the Dropping Strategy: Implementing the dropping strategy alone enhances the model's mIoU to 47.15%. This marginal improvement underscores the utility of selectively excluding low-quality frames to modestly boost model performance. (3) Crucial Role of the Boundary Strategy: The integration of the dropping and boundary strategies significantly elevates the model's mIoU to 74.47%. This substantial leap in performance highlights the boundary strategy's pivotal role in enhancing model accuracy by focusing on motion boundary supervision. (4) Incremental Benefit of the Variable Strategy: Incorporating all three strategies further increments the mIoU to 75.07%. This indicates that, beyond the significant gains achieved through the boundary strategy, fine-tuning the model with variable frame rates offers additional, albeit slight, enhancements to performance. This strategy fine-tunes the model by adapting the variability in frame rates, showcasing the nuanced improvements attainable through comprehensive optimization strategies.

Different Parameters of Boundary. According to Table 2 we can see that the Boundary method plays a crucial role. So we did some experiments on whether two of the key parameters affect the performance. We conducted 9 sets of experiments testing different degree thresholds with different dilation kernel sizes, and the results are shown in Table 3.

A brief analysis of our result gives us the following conclusions: (1) Impact of D Threshold on Performance: When the degree threshold is increased from $\frac{\pi}{12}$ to $\frac{\pi}{3}$, the mIoU performance of the model shows an overall improvement trend,

Table 2. Ablation study about three strategies to improve the baseline

	Metric		
Drop 1	Boundary	v Variable	mIoU(%)
			46.09
\checkmark			47.15
\checkmark	\checkmark		74.47
✓	\checkmark	\checkmark	75.07

Table 3. Different parameters of Boundary

Para	ameters	Metric
α	d	mIoU(%)
$\frac{\pi}{12}$	7	68.34
$\frac{\pi}{12}$	3	66.04
$\frac{\pi}{12}$	1	67.81
$\frac{\pi}{6}$	7	68.74
$\frac{\pi}{6}$	3	66.03
$\frac{\pi}{6}$	1	66.21
$\frac{\pi}{3}$	7	70.66
$\frac{\pi}{3}$	3	67.03
$\frac{\pi}{3}$	1	64.74

especially when the degree threshold is $\frac{\pi}{3}$ and the size of the dilation kernel is 7, the model achieves the highest mIoU performance (70. 66%), indicating that increasing the degree threshold can help improve the segmentation accuracy within a certain range. (2) The role of dilation kernel size: The dilation kernel size also affects the model performance, but this effect is related to the size of the degree threshold. At the same degree threshold, a dilation kernel size of 7 usually results in higher mIoU values, indicating that appropriately increasing the dilation kernel can better capture the boundary region and thus improve segmentation performance. (3) Combination of degree threshold and dilation kernel size: the best performance occurs in the configuration with a degree threshold of $\frac{\pi}{3}$ and a dilation kernel size of 7, suggesting that a reasonable choice of degree threshold and dilation kernel size is the key to improving the performance of the model segmentation when performing boundary extraction and enhancement.

4 Conclusion

In this study, we introduce a novel unsupervised surgical instrument segmentation approach that enhances model performance through direct boundary extraction from the optical stream, refined motion supervision via selective exclusion of low-quality frames, and a fine-tuning process incorporating variable frame rates. Evaluated using the MICCAI EndoVis 2017 VOS and Challenge datasets, our method demonstrates encouraging results, achieving an mIoU of 0.75 and 0.72, respectively. This indicates the method's capability to segment surgical instruments efficiently without reliance on manual annotations, potentially reducing the manual annotation burden in clinical environments and easing the annotation process for new datasets. The superiority and significance of our approach are further affirmed by comparisons with SOTA methods and an extensive ablation study. This paper not only introduces technological advancements but also highlights their practical value in clinical settings, paving the way for future research and application in the field.

References

- Bodenstedt, S., Wagner, M., Katić, D., Mietkowski, P., Mayer, B., Kenngott, H., Müller-Stich, B., Dillmann, R., Speidel, S.: Unsupervised temporal context learning using convolutional neural networks for laparoscopic workflow analysis. arXiv preprint arXiv:1702.03684 (2017)
- Bouget, D., Allan, M., Stoyanov, D., Jannin, P.: Vision-based and marker-less surgical tool detection and tracking: a review of the literature. Medical image analysis 35, 633-654 (2017)
- 3. DiPietro, R., Hager, G.D.: Unsupervised learning for surgical motion by learning to predict the future. In: International conference on medical image computing and computer-assisted intervention. pp. 281–288. Springer (2018)
- Dosovitskiy, A., Fischer, P., Ilg, E., Hausser, P., Hazirbas, C., Golkov, V., Van Der Smagt, P., Cremers, D., Brox, T.: Flownet: Learning optical flow with convolutional networks. In: Proceedings of the IEEE international conference on computer vision. pp. 2758–2766 (2015)
- 5. He, K., Zhang, X., Ren, S., Sun, J.: Deep residual learning for image recognition. In: Proceedings of the IEEE conference on computer vision and pattern recognition. pp. 770–778 (2016)
- 6. Jin, Y., Cheng, K., Dou, Q., Heng, P.A.: Incorporating temporal prior from motion flow for instrument segmentation in minimally invasive surgery video. In: Medical Image Computing and Computer Assisted Intervention—MICCAI 2019: 22nd International Conference, Shenzhen, China, October 13–17, 2019, Proceedings, Part V 22. pp. 440–448. Springer (2019)
- Lian, L., Wu, Z., Yu, S.X.: Bootstrapping objectness from videos by relaxed common fate and visual grouping. In: Proceedings of the IEEE/CVF Conference on Computer Vision and Pattern Recognition (CVPR). pp. 14582–14591 (June 2023)
- 8. Liao, Y., Kang, S., Li, J., Liu, Y., Liu, Y., Dong, Z., Yang, B., Chen, X.: Mobile-seed: Joint semantic segmentation and boundary detection for mobile robots. arXiv preprint arXiv:2311.12651 (2023)
- Liu, D., Wei, Y., Jiang, T., Wang, Y., Miao, R., Shan, F., Li, Z.: Unsupervised surgical instrument segmentation via anchor generation and semantic diffusion. In:
 Medical Image Computing and Computer Assisted Intervention–MICCAI 2020:
 23rd International Conference, Lima, Peru, October 4–8, 2020, Proceedings, Part III 23. pp. 657–667. Springer (2020)
- Liu, Y., Boels, M., Garcia-Peraza-Herrera, L.C., Vercauteren, T., Dasgupta, P., Granados, A., Ourselin, S.: Lovit: Long video transformer for surgical phase recognition. arXiv preprint arXiv:2305.08989 (2023)
- Liu, Y., Huo, J., Peng, J., Sparks, R., Dasgupta, P., Granados, A., Ourselin, S.: Skit: a fast key information video transformer for online surgical phase recognition. In: Proceedings of the IEEE/CVF International Conference on Computer Vision. pp. 21074–21084 (2023)
- 12. Mayer, N., Ilg, E., Hausser, P., Fischer, P., Cremers, D., Dosovitskiy, A., Brox, T.: A large dataset to train convolutional networks for disparity, optical flow, and scene flow estimation. In: Proceedings of the IEEE conference on computer vision and pattern recognition. pp. 4040–4048 (2016)
- 13. Ni, Z.L., Bian, G.B., Xie, X.L., Hou, Z.G., Zhou, X.H., Zhou, Y.J.: Rasnet: Segmentation for tracking surgical instruments in surgical videos using refined attention segmentation network. In: 2019 41st annual international conference of the IEEE engineering in medicine and biology society (EMBC). pp. 5735–5738. IEEE (2019)

- 14. Ni, Z.L., Zhou, X.H., Wang, G.A., Yue, W.Q., Li, Z., Bian, G.B., Hou, Z.G.: Surginet: Pyramid attention aggregation and class-wise self-distillation for surgical instrument segmentation. Medical Image Analysis **76**, 102310 (2022)
- 15. Psychogyios, D., Colleoni, E., Van Amsterdam, B., Li, C.Y., Huang, S.Y., Li, Y., Jia, F., Zou, B., Wang, G., Liu, Y., et al.: Sar-rarp50: Segmentation of surgical instrumentation and action recognition on robot-assisted radical prostatectomy challenge. arXiv preprint arXiv:2401.00496 (2023)
- Sestini, L., Rosa, B., De Momi, E., Ferrigno, G., Padoy, N.: Fun-sis: A fully unsupervised approach for surgical instrument segmentation. Medical Image Analysis 85, 102751 (2023)
- 17. Shi, X., Jin, Y., Dou, Q., Heng, P.A.: Semi-supervised learning with progressive unlabeled data excavation for label-efficient surgical workflow recognition. Medical Image Analysis 73, 102158 (2021)
- Shvets, A.A., Rakhlin, A., Kalinin, A.A., Iglovikov, V.I.: Automatic instrument segmentation in robot-assisted surgery using deep learning. In: 2018 17th IEEE international conference on machine learning and applications (ICMLA). pp. 624– 628. IEEE (2018)
- Teed, Z., Deng, J.: Raft: Recurrent all-pairs field transforms for optical flow. In: Computer Vision–ECCV 2020: 16th European Conference, Glasgow, UK, August 23–28, 2020, Proceedings, Part II 16. pp. 402–419. Springer (2020)
- Wan, J., Liu, Y., Wei, D., Bai, X., Xu, Y.: Super-bpd: Super boundary-to-pixel direction for fast image segmentation. In: Proceedings of the IEEE/CVF Conference on Computer Vision and Pattern Recognition (CVPR) (June 2020)
- Wei, M., Budd, C., Garcia-Peraza-Herrera, L.C., Dorent, R., Shi, M., Vercauteren, T.: Segmatch: A semi-supervised learning method for surgical instrument segmentation (2023)
- 22. Wu, Z., Lau, C.Y., Zhou, Q., Wu, J., Wang, Y., Liu, Q., Lei, Z., Liu, H.: Surgivisor: Transformer-based semi-supervised instrument segmentation for endoscopic surgery. Biomedical Signal Processing and Control 87, 105434 (2024)
- 23. Yang, L., Gu, Y., Bian, G., Liu, Y.: Tmf-net: A transformer-based multiscale fusion network for surgical instrument segmentation from endoscopic images. IEEE Transactions on Instrumentation and Measurement 72, 1–15 (2023). https://doi.org/10.1109/TIM.2022.3225922